



ELSEVIER

Nuclear Instruments and Methods in Physics Research A 475 (2001) 28–37

NUCLEAR
INSTRUMENTS
& METHODS
IN PHYSICS
RESEARCH
Section A

www.elsevier.com/locate/nima

Observation and analysis of self-amplified spontaneous emission at the APS low-energy undulator test line

N.D. Arnold^a, J. Attig^a, G. Banks^a, R. Bechtold^a, K. Beczek^a, C. Benson^a, S. Berg^a, W. Berg^a, S.G. Biedron^a, J.A. Biggs^a, M. Borland^a, K. Boerste^a, M. Bosek^a, W.R. Brzowski^a, J. Budz^a, J.A. Carwardine^a, P. Castro^b, Y.-C. Chae^a, S. Christensen^a, C. Clark^a, M. Conde^c, E.A. Crosbie^a, G.A. Decker^a, R.J. Dejus^a, H. DeLeon^a, P.K. Den Hartog^a, B.N. Deriy^a, D. Dohan^a, P. Dombrowski^a, D. Donkers^a, C.L. Doose^a, R.J. Dortwegt^a, G.A. Edwards^a, Y. Eidelman^a, M.J. Erdmann^a, J. Error^a, R. Ferry^a, R. Flood^a, J. Forrestal^a, H. Freund^d, H. Friedsam^a, J. Gagliano^a, W. Gai^c, J.N. Galayda^a, R. Gerig^a, R.L. Gilmore^a, E. Gluskin^a, G.A. Goepfner^a, J. Goetzen^a, C. Gold^a, A.J. Gorski^a, A.E. Grelick^a, M.W. Hahne^a, S. Hanuska^a, K.C. Harkay^a, G. Harris^a, A.L. Hillman^a, R. Hogrefe^a, J. Hoyt^a, Z. Huang^a, J.M. Jagger^a, W.G. Jansma^a, M. Jaski^a, S.J. Jones^a, R.T. Keane^a, A.L. Kelly^a, C. Keyser^a, K.-J. Kim^a, S.H. Kim^a, M. Kirshenbaum^a, J.H. Klick^a, K. Knoerzer^a, R.J. Koldenhoven^a, M. Knott^a, S. Labuda^a, R. Laird^a, J. Lang^a, F. Lenkszus^a, E.S. Lessner^a, J.W. Lewellen^a, Y. Li^a, R.M. Lill^a, A.H. Lumpkin^a, O.A. Makarov^a, G.M. Markovich^a, M. McDowell^a, W.P. McDowell^a, P.E. McNamara^a, T. Meier^a, D. Meyer^a, W. Michalek^a, S.V. Milton^{c,*}, H. Moe^a, E.R. Moog^a, L. Morrison^a, A. Nassiri^a, J.R. Noonan^a, R. Otto^a, J. Pace^a, S.J. Pasky^a, J.M. Penicka^a, A.F. Pietryla^a, G. Pile^a, C. Pitts^a, J. Power^c, T. Powers^a, C.C. Putnam^a, A.J. Puttkammer^a, D. Reigle^a, L. Reigle^a, D. Ronzhin^a, E.R. Rotela^a, E.F. Russell^a, V. Sajaev^a, S. Sarkar^a, J.C. Scapino^a, K. Schroeder^a, R.A. Seglem^a, N.S. Sereno^a, S.K. Sharma^a, J.F. Sidarous^a, O. Singh^a, T.L. Smith^a, R. Soliday^a, G.A. Sprau^a, S.J. Stein^a, B. Stejskal^a, V. Svirtun^a, L.C. Teng^a, E. Theres^a, K. Thompson^a, B.J. Tieman^a, J.A. Torres^a, E.M. Trakhtenberg^a, G. Travish^a, G.F. Trento^a, J. Vacca^a, I.B. Vasserman^a, N.A. Vinokurov^e, D.R. Walters^a, J. Wang^a, X.J. Wang^f, J. Warren^a, S. Wesling^a, D.L. Weyer^a, G. Wiemerslage^a, K. Wilhelmi^a, R. Wright^a, D. Wyncott^a, S. Xu^a, B.-X. Yang^a, W. Yoder^a, R.B. Zabel^a

*Corresponding author. Advanced Photon Source, Argonne National Laboratory, Argonne, IL 60439, USA.
E-mail address: milton@aps.anl.gov (S.V. Milton).

^a Advanced Photon Source, Argonne National Laboratory, Argonne, IL 60439, USA

^b Deutsches Elektronen-Synchrotron DESY, Notkestrasse 85, Hamburg 22603, Germany

^c Argonne Wakefield Accelerator, Argonne National Laboratory, Argonne, IL 60439, USA

^d Science Applications International Corporation, 1710 Goodridge Drive, McLean, VA 22102, USA

^e Budker Institute of Nuclear Physics, Novosibirsk 630090, Russian Federation

^f Brookhaven National Laboratory, Upton, NY 11973, USA

neous
line

Benson^a,
Boerste^a,
J.-C. Chae^a,
R.J. Dejus^a,
browski^a,
delman^a,
Freund^d,
Gilmore^a,
E. Grelick^a,
Iman^a,
Jaski^a,
Kim^a,
I. Knott^a,
Jewellen^a,
Kovch^a,
Meyer^a,
Nassiri^a,
Pietryla^a,
Rimmer^a,
Sajaev^a,
Sheno^a,
A. Sprau^a,
Thompson^a,
Trento^a,
Wang^a,
Wilhelmi^a,
Zabel^a

Abstract

Exponential growth of self-amplified spontaneous emission at 530 nm was first experimentally observed at the Advanced Photon Source low-energy undulator test line in December 1999. Since then, further detailed measurements and analysis of the results have been made. Here, we present the measurements and compare these with calculations based on measured electron beam properties and theoretical expectations. © 2001 Elsevier Science B.V. All rights reserved.

PACS: 41.60.Cr; 52.75.Va; 41.75.Lx; 29.27.-a

Keywords: Free-electron laser; Self-amplified spontaneous emission

1. Introduction

Third-generation synchrotron-light sources such as the Advanced Photon Source (APS) at Argonne National Laboratory currently provide high-brightness X-ray beams to a wide range of users. These sources rely on the spontaneous emission of synchrotron radiation generated by electron bunches passing through undulator magnets. Due to the incoherent nature of the emission process between individual electrons, the intensity of the generated light is proportional to the total number of particles within the bunch. This situation can be improved dramatically by forcing the electrons to emit coherently. In such a case, the intensity is proportional to the square of the total number of coherently radiating electrons. This is the underlying essence of current thought when speaking of the “next” or “fourth-generation” of synchrotron radiation sources.

Present plans for fourth-generation synchrotron radiation facilities capitalize on the self-amplified spontaneous emission (SASE) process [1,2] to induce the required microbunching within the electron bunch needed for coherent emission. The advantage of this process is that it does not require mirrors or an input seed, but starts up naturally from spontaneous noise. The process is thus scalable to X-ray wavelengths.

Until recently, SASE had only been observed at 633 nm and longer wavelengths [3–6]. The requirements on the electron beam properties become increasingly stringent as the wavelength is reduced; however, significant progress has been made in electron beam production technology and beam control such that the attainment of SASE into the vacuum ultraviolet (VUV) and perhaps soft X-ray wavelength range is becoming feasible. Progress in the study of SASE at these wavelengths will be used to guide the design of X-ray facilities utilizing the SASE effect [7–9]. We report here on recent progress in the study of SASE at 530 nm using the Low-Energy Undulator Test Line (LEUTL) facility at the APS, and briefly describe our future plans with the system.

2. LEUTL description

2.1. Overview

The APS linac and LEUTL systems have been configured as a test bed for SASE research and development at wavelengths ranging from the visible into the VUV. Upgrades to the linac have included the addition of radiofrequency (RF) electron guns for high-brightness electron beam generation, improvements in the magnetic lattice

structure, and performance upgrades of the RF modulators, low-level RF systems, and some power supplies [10]. The LEUTL is a 50-m tunnel in line with the linac and is capable of housing undulators or strings of undulators of over 30 m in length. The APS LEUTL system is designed to test concepts critical to the success of a linac-based fourth-generation light source, such as the proposed X-ray Linac Coherent Light Source (LCLS) at SLAC [9] and the TESLA-FEL at DESY [8], but at much longer wavelengths. Fig. 1 shows a schematic of the LEUTL SASE system and Table 1 lists the parameters for the first three phases of the operation.

2.2. Parameters

We have chosen to concentrate our initial efforts on investigation of SASE at 530 nm. Optics and optical diagnostics at this wavelength are readily available, the required electron beam performance at 217 MeV is readily achievable, and it is well within the operating envelope of the APS linac. As performance is improved, the energy of the electron beam will be increased to explore SASE at shorter wavelengths (see Table 1).

Table 1
LEUTL SASE design parameters for various phases of operation

	Phase 1	Phase 2	Phase 3
Wavelength (nm)	530	120	59
Electron energy (MeV)	217	457	650
Normalized rms emittance (μm)	5	3	3
Energy spread rms (%)	0.1	0.1	0.1
Peak current (A)	100	300	500
Undulator period (cm)	3.3	3.3	3.3
Magnetic field (T)	1.0	1.0	1.0
Undulator gap (mm)	9.3	9.3	9.3
Length of one undulator (m)	2.4	2.5	2.4
Power gain length (m)	0.81	0.72	0.77
Installed undulator length (m)	5×2.4	9×2.4	9×2.4
	then 9×2.4		

2.3. Linac

A schematic of the APS linac is shown in Fig. 2. It consists of 13 S-band, 3-m-long, constant gradient, travelling wave accelerating structures similar to the SLAC design. Three 35-MW klystrons each power four 3-m accelerating structures through a SLED. A photocathode gun (PC

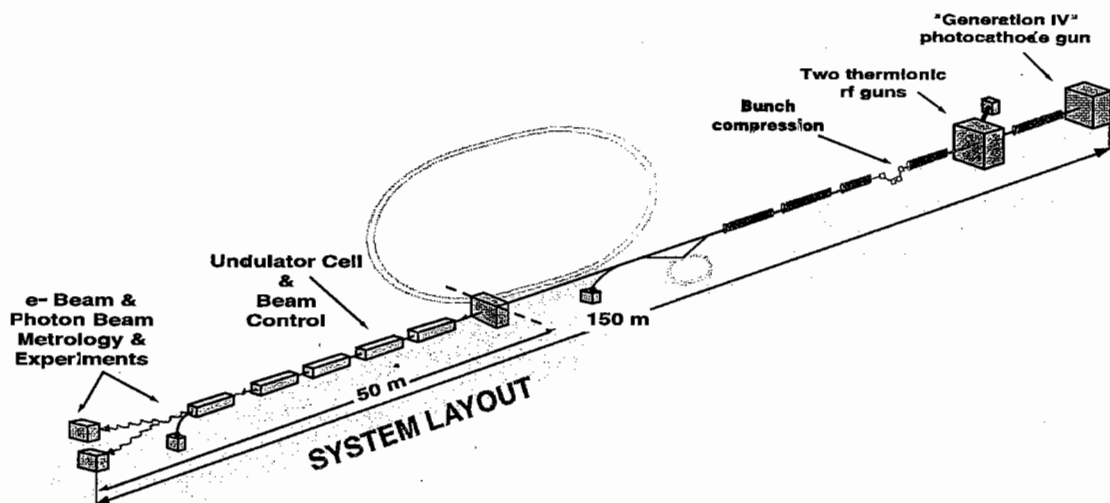


Fig. 1. Schematic of the APS LEUTL system.

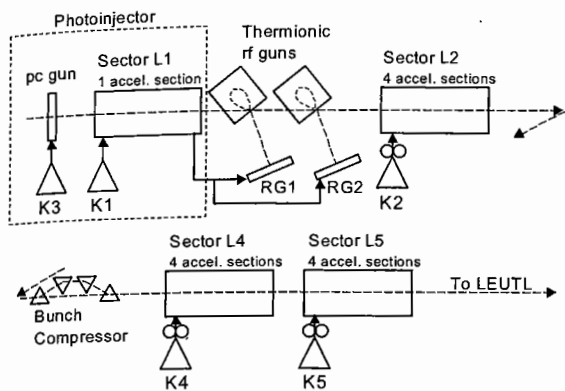


Fig. 2. Schematic of the APS linac system.

a 6-Hz repetition rate. The thermionic RF gun is a 1.5 cell S-band gun with a tungsten dispenser cathode. An alpha magnet is used to both inject beam into the APS linac and to compress the bunch to very high peak currents. An 8-ns pulsed kicker magnet is used for safety purposes to limit the total charge delivered to the linac. The result is a bunch train of roughly 23 bunches, each with approximately 48 pC of charge. This thermionic RF gun system is extremely reliable and is used as the primary injector for the APS storage ring.

2.5. Undulators

The undulator system is built of identical cells. Each cell contains a fixed-gap 2.4-m-long undulator with a 3.3-cm period and an undulator parameter, *K*, of 3.1. There is a diagnostic station, a horizontal focusing quadrupole, and horizontal and vertical steering before the first undulator, between each of the currently installed five undulators, and after the final undulator. The longitudinal spacing between undulators, about 0.38 m, is set to insure proper phase matching of the optical fields and the electron beam at successive undulator sections. In its current configuration of five cells, the total installed undulator magnetic length is 12 m.

2.6. Diagnostic arrangement

Direct measurement of the exponential growth of the optical intensity as a function of length along the undulator is a hallmark of our diagnostics design. Fig. 3 is a representative diagram of the diagnostics station located between each undulator. Electron beam diagnostics include YAG and optical transition radiation (OTR) screens viewed by a CCD camera. Two sets of filter wheels afford both intensity and, to a coarse degree, wavelength selectivity. Completing the primary electron beam diagnostics at each station are capacitive pickup beam position monitors (BPMs) with single-shot resolution of less than 10 μm for bunch charges of 1 nC.

In-tunnel visible light detectors (VLDs) consist of three-position actuators with positions as

gun) is powered by a single 35-MW klystron, while either of two thermionic RF guns share power with a single accelerating structure that follows the photocathode RF gun. Power distribution to these RF guns and linac structure is through S-band RF switches. In the PC gun mode, the electron beam can be accelerated by all 13 structures. The maximum energy attainable in PC gun mode is 650 MeV. One accelerating structure, the first, is not used to accelerate beam in the thermionic RF gun configuration.

A bunch compression system has recently been installed and commissioned within the linac following the fifth accelerating structure [11,12]. It will provide higher peak currents for both photocathode and thermionic RF guns. It was, however, not installed during the measurements reported here.

2.4. Guns

High-brightness electron bunches are generated using either a photocathode RF gun system or a thermionic RF gun with alpha-magnet compression. The photocathode RF gun is a 1.6-cell Brookhaven S-band gun IV model [6,13] that employs a copper photocathode. A Nd:glass picosecond drive laser system is used to generate the electrons [14]. It is assembled from commercially available components and is timing stabilized to the RF within 1 ps. This system can generate a single electron bunch of roughly 1 nC at

ious phases of

Phase 2	Phase 3
20	59
57	650
	3
1	0.1
0	500
3	3.3
0	1.0
3	9.3
5	2.4
2	0.77
2.4	9 × 2.4

n in Fig. 2.
constant
structures
e 35-MW
iting struc-
e gun (PC

un



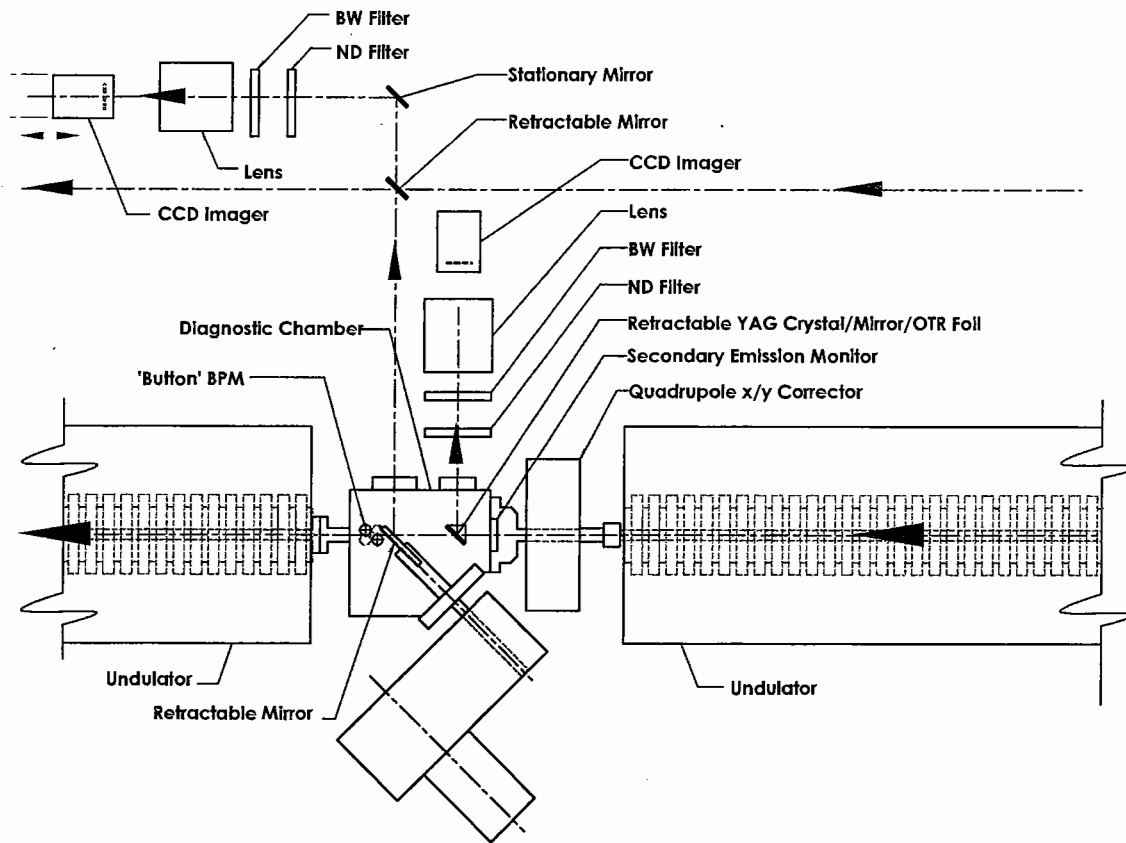


Fig. 3. Schematic of the undulator diagnostic stations.

follows: (1) out, (2) mirror, (3) mirror with 600- μm diameter hole. These are used to deflect the synchrotron light through a set of filters to a CCD camera. All five mirror hole centers have been aligned along the beamline to within 20 μm of the ideal electron beam trajectory. The cameras viewing these mirrors can be focused at the mirror, at infinity, or at any distance between the two. Focus at infinity is valuable as it allows us to measure the angular distribution of the optical radiation.

A green alignment laser is located at the entrance to the undulator string. It is used to insure that all mirrors and optical components are properly aligned. It also serves as an intensity and wavelength calibration source for the optical systems.

Further details of the LEUTL system, the undulators, and the diagnostics arrangements can be found in Refs. [15–19].

3. Gain analysis

3.1. Via fitted intensity growth

Measurements of the signal intensity as a function of length along the undulator can be used to extract the SASE gain length. In the SASE FEL, the Fourier harmonics of the field amplitude $E_\omega(s, z)$ at frequency ω grow exponentially with position along the undulator z :

$$E_\omega(s, z) \propto \exp(gz) \quad (1)$$

where s is the position along the bunch. Near the optimal frequency ω_0 at the point s_0 within the bunch, where the longitudinal particle density is maximal, the factor g reaches a maximum, and therefore, can be represented in the form

$$g \approx \frac{1}{2L_G} [1 - a(\omega - \omega_0)^2 - b(s - s_0)^2] \quad (2)$$

where L_G is the power gain length at the optimal frequency and peak current, and a and b are constants.

The radiated energy W is then proportional to

$$W \propto \int_{-\infty}^{\infty} \int_{-\infty}^{\infty} |E_{\omega}(s, z)|^2 ds d\omega$$

$$\approx \frac{L_G}{z} \exp\left(\frac{z}{L_G}\right) \frac{\pi}{\sqrt{ab}} \quad (3)$$

Thus, W can be written in the form

$$W(A, L_G, z) \approx A \frac{L_G}{z} \exp\left(\frac{z}{L_G}\right). \quad (4)$$

The quantities L_G and A can be explicitly calculated in terms of the electron beam and undulator parameters [20–25].

3.2. Via opening angle

An alternative, albeit rough, way of determining the gain length is by observation of the opening angle of the optical radiation. An estimate of the gain length based on the FWHM angular divergence of the SASE radiation θ_{SASE} is

$$L_G \approx 2\lambda_r / \pi\theta_{\text{SASE}}^2 \quad (5)$$

where λ_r is the observed resonant wavelength.

3.3. Intensity fluctuations

Intensity fluctuations of the optical signal are intrinsic to the SASE process [26,27]. This is due to the startup from noise developing into a number of longitudinal degrees of freedom within the resultant optical pulse. Roughly, the number of degrees of freedom is

$$M = \frac{\pi \sigma_{\ell} \lambda_u}{2 \lambda_r z} \quad (6)$$

where σ_{ℓ} is the rms electron bunch length, z is the length of the “exponential-growth” part of the undulator (the observation point along the undulator minus approximately two power gain lengths), and λ_u is the undulator period. Eq. (6) is valid for $M > 1$. The standard deviation of the shot-to-shot fluctuations is found to be equal to $1/\sqrt{M}$.

Although one clearly observes these fluctuations, their use for precise quantitative measurement of the SASE process is hindered by a lack of precise knowledge of the beam properties. This is further exacerbated by shot-to-shot fluctuation of the electron beam properties.

4. Gain measurements

4.1. Early data

4.1.1. Measured gain

First measurement of significant SASE using the PC gun was on December 22, 1999 [28]. Fig. 4 shows the optical intensity following the first four undulators. The signal is the integral over all measurable angles, within a 10-nm bandwidth, and over the duration of the electron bunch. At the time of the measurement, there was significant shot-to-shot fluctuation in the beam properties and trajectory. As a result, we plot the peak

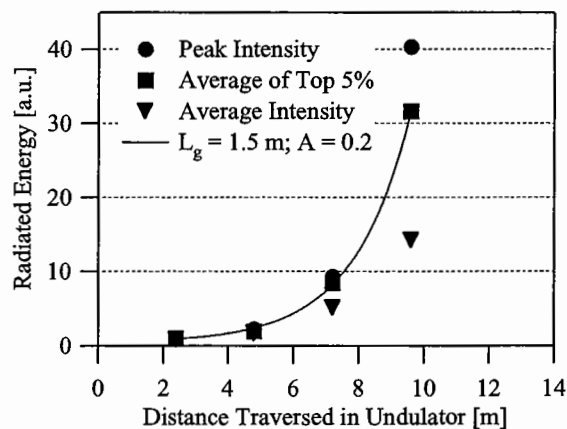


Fig. 4. Early data. Radiated energy vs. distance traversed in the undulator. The PC gun source was used for this experiment.

Table 2
Measured linac beam parameters at the end of the linac using beam from the PC gun on December 22nd

	Typical	Min-Max
Energy (MeV)	217	—
Normalized emittance (μm)	5	4–8
Charge/bunch (nC)	0.7	0.6–0.8
Bunch length FWHM (ps)	5	4–7
Energy spread rms %	0.1	<0.1–0.2

measured intensity, the average of the top 5% measured intensities, and the average of all measurements at each diagnostic station. All measurements were taken with the electron beam properties shown in Table 2.

By fitting the average of the top 5% to the functional form given in Eq. (4), we found a gain length of 1.5 m. Similarly, the opening angle of the SASE signal following the fourth undulator implies, from Eq. (5), a gain length of 1.6 m.

The theoretical gain length, using the typical values listed in Table 2 and calculated by methods discussed in Refs. [20–25], is 0.7 m. The discrepancy between theory and the experimentally measured values was probably due to incomplete knowledge of the electron beam parameters.

4.2. Thermionic RF gun data

4.2.1. Beam properties

Fig. 5 shows SASE signal measurements as a function of length along the undulator system using beam from a high performance thermionic RF gun system. Electron bunches from the thermionic RF gun were optimally compressed by the alpha magnet by observing signals generated off a coherent transition radiation bunch length monitor [29]. Reconstruction of the longitudinal bunch profile was performed with the result tabulated in Table 3. Also shown in Table 3 are the measured electron beam properties for this experiment. Sequential measurements at each undulator diagnostics station were made for a number of electron bunches. Shown are the averages of all measurements. The intensity measured is an integration over all wavelengths, angles, and the duration of the electron bunch.

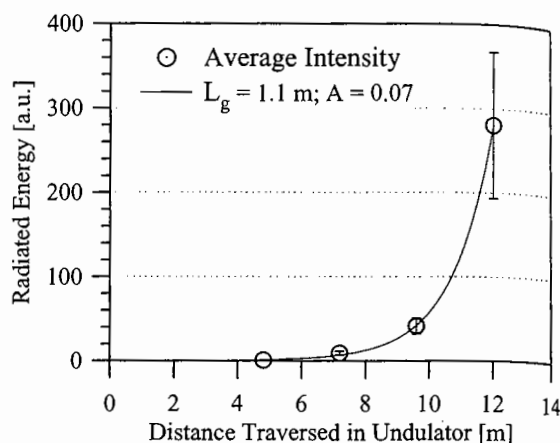


Fig. 5. Radiated energy vs. distance traversed in the undulator. Thermionic RF gun source.

Table 3
Measured linac beam parameters at the end of the linac using beam from the thermionic RF gun

	Typical	Min-Max
Energy (MeV)	217	—
Normalized emittance (μm)	12	9–15
Charge/bunch (nC)	0.048	0.043–0.052
Bunch length FWHM (ps)	0.35	0.33–0.40
Energy spread rms %	0.1	<0.1–0.2

With this electron source the intensity signal is also an integral over the entire 23-bunch train generated during each linac macropulse. Error bars correspond to the rms fluctuation of the measured intensity signal. Fitting to the average value of the measured signal gives a gain length of 1.1 m.

As before, one can calculate the expected gain lengths. Using the typical values from Table 3, a gain length of 1.0 m is calculated. A more complete Monte Carlo analysis using normalized three-point estimates based on the beam parameters listed in the table predicts a most probable gain length of 1.1 m with a distribution width of ± 0.2 m, which is in good agreement with the measured data.

4.2.2. Fluctuations

It is interesting to note that at 530 nm, the FWHM length of the thermionic gun electron

bunch
and th
length
Eq. (6
to be
avera
woul
 $1/\sqrt{2}$
nearl
electr

4.3.

4.3.1

Fi
2000
inclu
point
the
mea
inte
dur:
nor
und
not
the
thi

bunch corresponds to roughly 200 optical periods and the undulator is 360 periods long. The bunch length is then less than the slippage length and Eq. (6) is not valid. M can, therefore, be assumed to be close to 1. Given that each measurement is an average over the 23 bunches in the bunch train, we would expect fluctuations in the intensity of $1/\sqrt{23} \approx 20\%$. Our data indicate fluctuations of nearly 30%, indicating that fluctuations in the electron beam properties were dominant.

4.3. Recent PC gun data

4.3.1. Measured gain

Fig. 6 shows our most recent data taken in July 2000 using the beam from the PC gun. Also included in the figure is the fit to Eq. (4). The data points are the average of all measurements, and the error bars indicate the rms spread in the measurements. Once again the intensity is an integration over all wavelengths, angles, and the duration of the electron bunch. All data were normalized to the intensity following the second undulator. Data following the first undulator were not used in order to insure that we were well into the exponential-growth regime. Data following the third undulator are missing due to problems

encountered with the diagnostics system at this location.

4.3.2. Comparison to theory

Table 4 lists the beam conditions for all three run conditions shown in Fig. 6. Also listed are the fitted and predicted gain lengths for the listed beam conditions. The agreement is very good. The total installed length of undulator at the time of these measurements was 12 m. For a gain length of 0.8 m, this would imply that 15 gain lengths have been traversed.

Further confirmation of the gain length comes from measurement of the opening angle. We measured an FWHM opening angle following the fourth undulator of approximately $600 \mu\text{rad}$, in agreement with the angular divergence of the fundamental guided mode obtained by solving the eigenmode equation [23]. From Eq. (5), this implies a gain length of 0.9 m, again in rough agreement with the measurement of 0.8 m.

Error bars in Fig. 6 indicate the rms spread in the measured intensity. Measured spreads of the intensity signals at the last two diagnostics stations are in the order of 50–60%. Electron bunch lengths were $300 \mu\text{m}$ rms. For our parameters, M

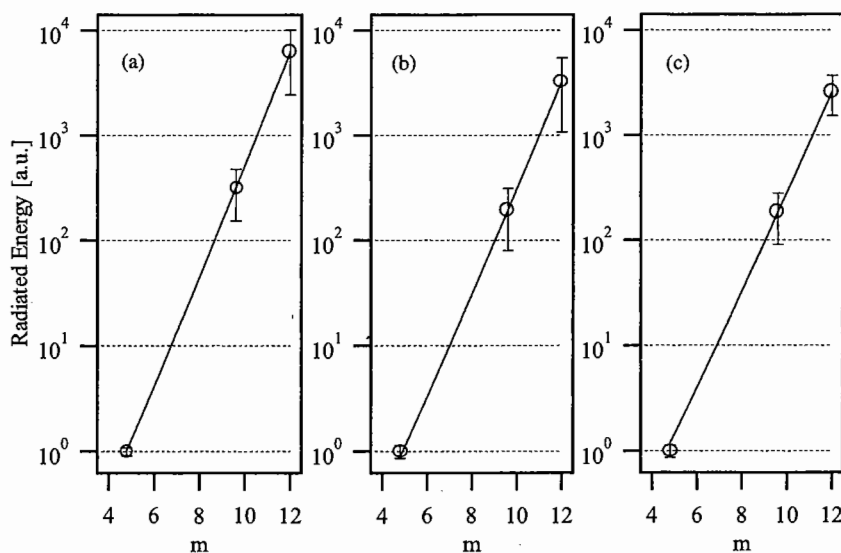


Fig. 6. Radiated energy vs. distance along undulator for the three run conditions listed in Table 4.

Table 4
Beam measurements, fitted gain length, and calculated gain lengths for the data displayed in Fig. 6^a

	A	B	C
Peak current (A)	170	130	150
Charge (nC)	0.42	0.45	0.50
Normalized emittance (π mm-mrad)	9	7.5	7.5
Fitted gain length (m)	0.75	0.80	0.82
Calculated gain length (m)	0.77	0.83	0.76

^aNote: rms energy spread $\sim 0.1\%$ for all cases.

is calculated to be 2.4, giving an expected fluctuation level of 64%.

4.4. Confirmation of beam bunching

As further confirmation of microbunching, we observed the OTR evolution to coherent transition radiation (CTR) as a function of distance along the undulator. The synchrotron radiation signal was blocked by a thin foil immediately preceding the 45° metal pickoff mirror [30]. The resultant CTR signal was then directed to the wall-mounted VLD camera system, and in the case of the fifth

undulator, it could also be transported to an optical spectrometer. A 530-nm filter was used for the VLD measurements to insure that we viewed the CTR signal at the expected bunching wavelength. Although the CTR signals as measured at the VLDs have not been fully analyzed, they do show indication of intensity gains well beyond linear. Perhaps the most significant signature of bunching, though, was via the spectrometer measurements that showed a CTR narrow-band signal at the SASE fundamental wavelength (Fig. 7).

5. Summary

Exponential growth of the optical signal as a function of length has been directly measured at 530 nm, providing clear evidence of the SASE process. Early measurements made using beam from the photocathode RF gun indicated a gain length of 1.5 m. This was later improved to 0.8 m in agreement with theory, giving a total of 15 power gain lengths within our undulator system. A thermionic RF gun with alpha-magnet compres-

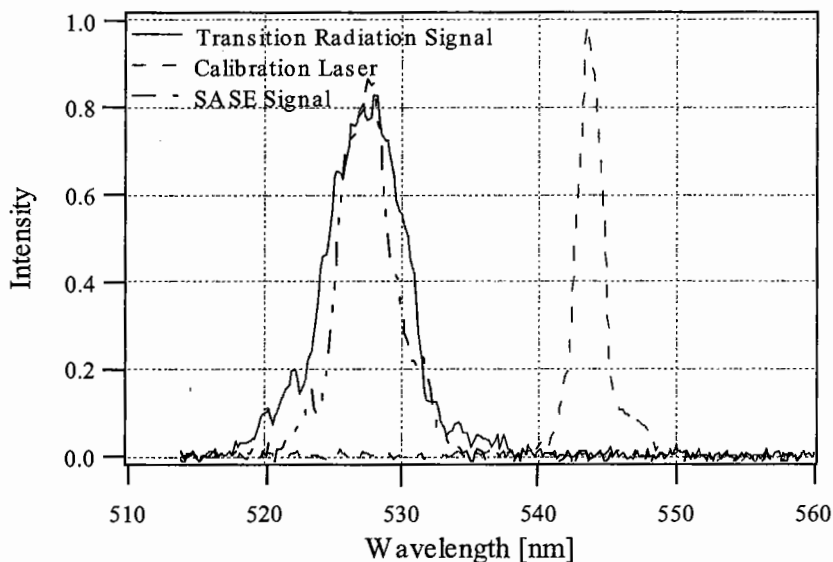


Fig. 7. CTR spectrum of the microbunched beam along with the SASE spectrum at the same location. The intensities were adjusted with neutral density filters to be roughly equal. (The SASE is ~ 200 times brighter.) The data were not taken simultaneously. The sharp line at 543.5 nm is the calibration laser.

sion has also been used and a gain length as low as 1.1 m at 530 nm was measured. Initial measurements of electron beam microbunching at the resonant wavelength also provide strong evidence of the SASE process. Measurements of the gain length now agree with the theoretical predictions, but we are still suffering from fluctuations in the electron beam properties.

We have recently installed a bunch compression system into the APS linac and are in the early stages of commissioning it. Four additional undulators are also being installed, which will bring the total length of installed undulator to 21.6 m. With this setup, we will explore SASE at and beyond saturation. We will also investigate nonlinear harmonic generation [31] and increase the beam energy of the linac to begin exploration of SASE at even shorter wavelengths.

Acknowledgements

This work is supported by the U.S. Department of Energy, Office of Basic Energy Sciences, under Contract No. W-31-109-ENG-38.

References

- [1] Y.S. Derbenev, A.M. Kondratenko, E.L. Saldin, Nucl. Instr. and Meth. 193 (1982) 415.
- [2] R. Bonifacio, C. Pellegrini, L.M. Narducci, Opt. Commun. 50 (1985) 6.
- [3] T.J. Orzechowski, et al., Nucl. Instr. and Meth. A 250 (1986) 144.
- [4] D.A. Kirkpatrick, et al., Phys. Fluids B 1 (7) (1989) 1511.
- [5] M. Hogan, et al., Phys. Rev. Lett. 81 (1998) 4807.
- [6] M. Babzien, et al., Phys. Rev. E 57 (1998) 6093.
- [7] R. Tatchyn, et al., Nucl. Instr. and Meth. A 374 (1996) 274.
- [8] R. Brinkmann, G. Materlik, J. Rossbach, A. Wagner (Eds.), Conceptual design of a 500 GeV e^+e^- linear collider with integrated X-ray laser facility, DESY Report No. DESY97-048, 1997.
- [9] M. Cornacchia, et al., Linac Coherent Light Source (LCLS) Design Study Report, Stanford University, University of California Report No. SLAC-R-521 / UC-414, revised 1998.
- [10] Travish, et al., High-brightness beams from a light source injector: the advanced photon source low-energy undulator test line linac, in: A. Chao (Ed.), Proceedings of the 20th International Linac Conference, SLAC-R-561 (CD available from the Stanford Linear Accelerator Center, Stanford, CA, 2000).
- [11] M. Borland, Design and performance simulations of the bunch compressor for the APS LEUTL FEL, in: A. Chao (Ed.), Proceedings of the 20th International Linac Conference, SLAC-R-561 (CD available from the Stanford Linear Accelerator Center, Stanford, CA, 2000).
- [12] M. Borland, J. Lewellen, S. Milton, A highly flexible bunch compressor for the APS LEUTL FEL, in: A. Chao (Ed.), Proceedings of the 20th International Linac Conference, SLAC-R-561 (CD available from the Stanford Linear Accelerator Center, Stanford, CA, 2000).
- [13] S. Biedron, et al., in: Proceedings of the 1999 Particle Accelerator Conference, IEEE Press, New York, 1999, pp. 2024–2026.
- [14] G. Travish, N. Arnold, R. Koldenhoven, in: J. Feldhaus, H. Weise (Eds.), Free Electron Lasers 1999, Vol. II, Elsevier, Amsterdam, 2000, p. 101.
- [15] S.V. Milton, et al., Nucl. Instr. and Meth. A 407 (1998) 210.
- [16] S.V. Milton, et al., Proc. SPIE Int. Soc. Opt. Eng. 3614 (1999) 86.
- [17] I.B. Vasserman, et al., in: Proceedings of the 1999 Particle Accelerator Conference, IEEE Press, New York, 1999, pp. 2489–2491.
- [18] I.B. Vasserman, N.A. Vinokurov, R.J. Dejus, Phasing of the insertion devices at APS FEL Project, Proceedings of the 11th National Conference on Synchrotron Radiation Instrumentation, Stanford, CA, 1999; AIP Conference Proceedings, Vol. 521, Melville, New York, 2000, pp. 368–371.
- [19] E. Gluskin, et al., Nucl. Instr. and Meth. A 429 (1999) 358.
- [20] L.-H. Yu, S. Krinsky, R.L. Gluckstern, Phys. Rev. Lett. 64 (1990) 3011.
- [21] Y.H. Chin, K.-J. Kim, M. Xie, Phys. Rev. A 46 (1992) 6662.
- [22] M. Xie, in: Proceedings of the 1995 Particle Accelerator Conference, IEEE, Dallas, 1995, pp. 183–185.
- [23] M. Xie, Exact and variational solutions of 3D eigenmodes for high-gain FELs, Nucl. Instr. and Meth. A 445 (2000) 59.
- [24] M. Xie, Nucl. Instr. and Meth. A 475 (2001) 51, these proceedings.
- [25] Z. Huang, K.-J. Kim, Nucl. Instr. and Meth. A 475 (2001) 59, these proceedings.
- [26] R. Bonifacio, et al., Phys. Rev. Lett. 73 (1994) 70.
- [27] E.L. Saldin, E.A. Schneidmiller, M.V. Yurkov, DESY Report TESLA-FEL 97-02, 1997.
- [28] S.V. Milton, et al., Phys. Rev. Lett. 85 (2000) 988.
- [29] A. Lumpkin, et al., Nucl. Instr. and Meth. A 429 (1999) 336.
- [30] A.H. Lumpkin, et al., Nucl. Instr. and Meth. A 475 (2001) 462, these proceedings.
- [31] H.P. Freund, S.G. Biedron, S.V. Milton, Nucl. Instr. and Meth. A 445 (2000) 53.

ported to an
was used for
at we viewed
bunching wave-
s measured at
ized, they do
well beyond
signature of
spectrometer
narrow-band
wavelength

l signal as a
measured at
f the SASE
using beam
cated a gain
ved to 0.8 m
total of 15
or system. A
et compres-

were adjusted
ly. The sharp